# On the Modeling of Snowflake Growth Using Hexagonal Automata

*Jessica Li, MIT PRIMES-USA and Illinois Geometry Lab*

*Mentor: Professor Laura Schaposnik*

## Abstract

Snowflake growth is an example of crystallization, a basic phase transition in physics. Studying snowflake growth helps gain fundamental understanding of this basic process and may help produce better crystalline materials and benefit several major industries. The basic theoretical physical mechanisms governing the growth of snowflake are not well understood: whilst current computer modeling methods can generate snowflake images that successfully capture some basic features of actual snowflakes, so far there has been no analysis of these computer models in the literature, and more importantly, certain fundamental features of snowflakes are not well understood. A key challenge of analysis is that the snowflake growth models consist of a large set of partial difference equations, and as in many chaos theory problems, rigorous study is difficult. In this paper we analyze a popular model (Reiter's model) using a combined approach of mathematical analysis and numerical simulation. We divide a snowflake image into main branches and side branches and define two new variables (growth latency and growth direction) to characterize the growth patterns. We derive a closed form solution of the main branch growth latency using a one dimensional linear model, and compare it with the simulation results using the hexagonal automata. We discover a few interesting patterns of the growth latency and direction of side branches. On the basis of the analysis and the principle of surface free energy minimization, we propose a new geometric rule to incorporate

interface control, a basic mechanism of crystallization that is not taken into account in the original Reiter's model.

## 1. Introduction

Snowflakes exhibit a rich combination of characteristic symmetry and complexity. The six fold symmetry is a result of the hexagonal structure of the ice crystal lattice, and the complexity comes from the random motion of individual snow crystals falling through the atmosphere. Figure 1 shows different real snowflakes.

Figure 1. Plates and dendrites [5]. (a) Stellar dendrite (b) Stellar plate (c) Sectored plate.

Snowflake growth is a specific example of crystallization – how crystals grow and create complex structures. Because crystallization is a basic phase transition in physics, and crystals make up the foundation of several major industries, studying snowflake growth helps gain fundamental understanding of how molecules condense to form crystals. This fundamental knowledge may help fabricate new and better types of crystalline materials [4].

Scientific studies of snowflakes can be categorized into two main types. The first type takes a macroscopic view by observing natural snowflakes in a variety of morphological environments characterized by temperature, pressure and vapor density [6,7,8]. The second type takes a microscopic view and investigates the basic theoretical physical mechanisms governing the growth of snowflakes [4]. While some aspects of snowflake growth, e.g., the crystal structure of ice, are well understood, many other aspects such as diffusion limited growth are at best understood at a qualitative level [4]. Computer modeling [2,3,9,10,11,12] is yet another approach in which snowflake growth is numerically simulated to produce images with mathematical models derived from the physical principles. By comparing computer generated images with

actual snowflakes, one can correlate the mathematical models and their parameters with physical conditions.

While computer modeling can generate snowflake images that successfully capture some basic features of actual snowflakes, so far there has been no analysis of these computer models in the literature. Moreover, certain fundamental features of snowflakes are still not well understood. In this paper we attempt to analyze snowflake growth simulated by the computer models so as to connect the microscopic and macroscopic views and to further our understanding of snowflake physics. A key challenge of analysis is that the snowflake growth models (e.g., [2,11]) consist of a large set of partial difference equations and no analytical solution is known. The models that have been considered in the past are in essence chaos theory models, which is why they successfully capture the real world phenomena, but prove to be notoriously difficult to analyze rigorously. In this paper we analyze a popular model (Reiter's model [11]) using a combined approach of mathematical analysis and numerical simulation.

The rest of this paper is organized as follows. Section 2 summarizes Reiter's model. In Section 3 we divide a snowflake image into main branches and side branches, define growth latency and direction to characterize the growth patterns, and describe general geometric properties. In Section 4, we derive a new closed form solution of the main branch growth latency with a one dimensional linear model, and compare it with the simulation results. In Section 5, we study the growth latency and direction of side branches. On the basis of the analysis and the principle of surface free energy minimization, in Section 6, we propose a new geometric rule to incorporate interface control, a basic mechanism of crystallization that is not taken into account in the original Reiter's model. We summarize our contributions and present a few future work directions in Section 7.

## 2. An overview of Reiter's model

Reiter's model is a hexagonal automata which can be described as follows. Tessellate the plane into hexagonal cells. Each cell $z$ has six nearest neighbors. The state variable $s_t(z)$ of cell $z$ at time $t$ represents the amount of water stored in cell $z$. The cells are divided into three types:

**Definition 2.1** A cell $z$ is called *frozen* if $s_t(z) \geq 1$. If a cell is not frozen itself but at least one of the nearest neighbors is frozen, the cell is called a *boundary* cell. A cell that is neither frozen nor boundary is called *nonreceptive*. The union of frozen and boundary cells are called *receptive* cells.

Reiter's growth model starts from a single ice crystal $s_0(\mathbf{0}) := 1$ at the origin cell $\mathbf{0}$, which represents a thin hexagonal prism. For all other cells $s_0(z) := \beta$, where $\beta$ represents a fixed constant background vapor level. The state of a cell evolves as a function of the states of its nearest neighbors according to the local update rules that reflect the underlying mathematical models. To describe the local update rules, we use $^-$ and $^+$ notations to denote the variables before and after a step is completed. At time $t$, define two variables $u_t(z), v_t(z)$ of each cell $z$: $u_t(z)$ represents the amount of water that participates in diffusion, and $v_t(z)$ is the amount that does not participate. If cell $z$ is receptive, $u_t(z) := 0$ and $v_t(z) := s_t(z)$; otherwise, $u_t(z) := s_t(z)$ and $v_t(z) := 0$.

Given $\gamma, \alpha$ two fixed constants representing vapor addition and diffusion coefficients respectively, Reiter's model is based on the following two local update rules:

- *Constant addition*. For any receptive cell $z$,

$$v_t^+(z) := v_t^-(z) + \gamma. \tag{1}$$

- *Diffusion*. For any cell $z$,

$$u_t^+(z) := u_t^-(z) + \frac{\alpha}{2}\left(\bar{u}_t^-(z) - u_t^-(z)\right), \tag{2}$$

where $\bar{u}_t^-(z)$ is the average of $u_t^-$ for the six nearest neighbors of cell $z$.

The underlying physical principle of Equation (2) is the diffusion equation

$$\frac{\partial u}{\partial t} = a\nabla^2 u, \tag{3}$$

where $a$ is a constant and $\nabla^2 u = \frac{\partial^2 u}{\partial x^2} + \frac{\partial^2 u}{\partial y^2}$ is the Laplacian. Equation (2) is the discrete version of Equation (3) on the hexagonal lattice, and it states that cell $z$ keeps $\left(1 - \frac{\alpha}{2}\right)$ fraction of $u_t^-(z)$ to itself, uniformly distributes the remaining to its six neighbors, and receives $\frac{\alpha}{12}$ fraction from each neighbor. The total amount of $u_t(z)$ would be conserved within the entire system, except that a real world simulation consists of a finite number of contiguous cells. The cells at the edge of the simulation setup are referred to as *edge cells*, in which one sets $u_t^+(z) := \beta$. Thus, water is added to the system via the edge cells in the diffusion process.

Combining the two intermediate variables, one obtains

$$s_{t+1}(z) := u_t^+(z) + v_t^+(z). \tag{4}$$

By varying $\alpha, \beta, \gamma$, Reiter's model can generate certain geometric forms of snowflakes observed in nature. Figure 2 shows a variety of dendrite and plate forms generated from Reiter's model.

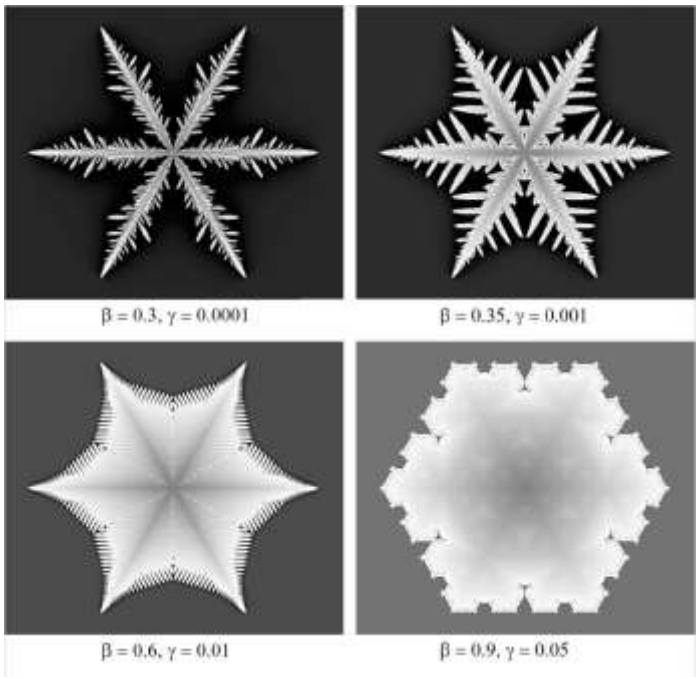


Figure 2. Snowflake images generated by Reiter's model published in [11], with $\alpha = 1$. The upper left figure is (a), the upper right figure is (b), the lower left figure is (c), and the lower right figure is (d).

## 3. General geometric properties

In what follows, we give new descriptions of snowflake growth and analyze them with a combined approach of mathematical analysis and numerical simulation. To model snowflake growth, we consider a coordinate system of cells as in Figure 3(a). A cell $z$ is represented by its coordinate $(i, j)$, for $i, j \in \boldsymbol{Z}$. Thanks to the six fold symmetry, we only focus on one twelfth of the cells, marked as dark dots, for which $j \geq i \geq 0$:

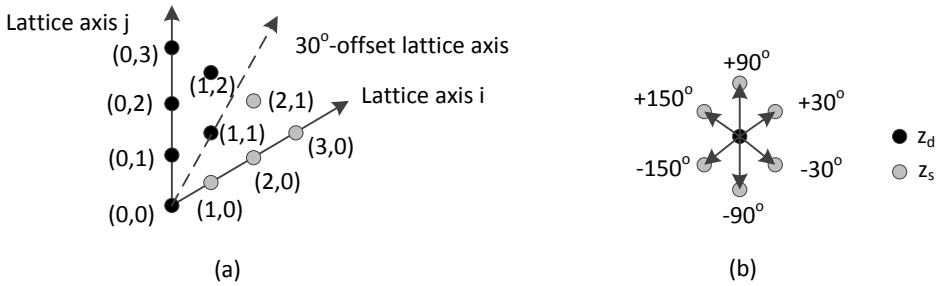


Figure 3. (a) Coordinate system of hexagonal cells. (b) Definition of growth directions in the coordinate system.

The images in Figure 2 show that a crystal consists of six main branches that grow along the lattice axes, and numerous side branches that grow from the main branches in a seemingly

random manner. The main and side branches exhibit a rich combination of characteristic symmetry and complexity. Before we analyze the growth pattern of the main and side branches, we can show the following general geometric properties.

**Definition 3.1** *The rate of water accumulation* of cell $z$ is defined as $\Delta s_t(z) = s_{t+1}(z) - s_t(z)$.

**Proposition 3.1** For a nonreceptive cell $z$, one has $0 < s_t(z) \leq \beta$ and $\Delta s_t(z) \leq 0$. Moreover, $s_t(z) = \beta$ only for edge cell $z$.

**Proposition 3.2** For a boundary cell $z$, $\Delta s_t(z)$ is the sum of $\gamma$ and diffusion. If $\gamma > 0$, there exists $t_0 > 0$ such that $s_{t_0}(z) \geq 1$; otherwise, $\lim_{t\to\infty} s_t(z) < 1$ if cell $z$ is surrounded by a set of frozen cells and disconnected from the edge cells.

**Proposition 3.3** For a frozen cell $z$, one has $\Delta s_t(z) = \gamma$.

**Proposition 3.4** At any time the set of all the receptive cells are connected. Moreover, suppose that a nonreceptive cell $z$ is surrounded by receptive cells and disconnected from the edge cells. If $\gamma > 0$, there exists $t_0 > 0$ such that $s_{t_0}(z) \geq 1$; otherwise, $\lim_{t\to\infty} s_t(z) < 1$.

To become frozen, a cell goes through two stages of growth. First, it is nonreceptive and loses vapor to other cells due to diffusion (Proposition 3.1). Next, it becomes boundary and accumulates water via diffusion and addition (Proposition 3.2) until it becomes frozen and sees no benefit of diffusion (see Proposition 3.3). Becoming boundary is a critical event between the two stages. We focus on the second stage and define two new variables to characterize growth patterns.

**Definition 3.2** The time to be frozen of a cell $z$ is denoted by $T(z)$ and defined by the condition $s_{T(z)}(z) \geq 1$, and $s_t(z) < 1$ for $t < T(z)$. Similarly, one can define $B(z)$ as the first time to be boundary. *Growth latency* is denoted by $L(z)$ and defined by $L(z) := T(z) - B(z)$.

A cell (referred to as destination cell $z_d$) becomes boundary as one of its neighboring cells (referred to as source cell $z_s$) has just become frozen. Note that while the growth of $z_d$ is traced back to a unique $z_s$, a source cell may correspond to multiple destination cells.

**Definition 3.3** *Growth direction* of cell $z_d$ is denoted by $g(z_d)$ and defined as the orientation of $z_s$ with respect to $z_d$. As shown in Figure 3(b), the angle is given relative to the horizontal direction in the coordinate system, and satisfies $g(z_d) \in \{+30°, -30°, +90°, -90°, +150°, -150°\}$. The source-destination cell relationship is denoted by $z_s = S(z_d)$.

## 4. Growth of main branches

The snowflake growth is fastest along a lattice axis, which represents a main branch. The growth is slowest along the 30°-offset lattice axis. More precisely, consider cells $(i, j)$ where $i + j = K$ for a fixed $K$. These cells are all $K$ hops from the origin $(0,0)$ on the grid. The main branch growth pattern is such that $T(0, K) \leq T(i, j)$ and that $T\left(\frac{K}{2}, \frac{K}{2}\right) \geq T(i, j)$ for even $K$ and $T\left(\frac{K-1}{2}, \frac{K+1}{2}\right) \geq T(i, j)$ for odd $K$. Along the lattice $j$-axis, $g(0, j) = -90°$ for all $j$.

We next develop a model to calculate the growth latency $L(0, j)$. Note that when cell $(0, j)$ becomes frozen, cell $(0, j + 1)$ becomes boundary immediately. It follows that the first time to be boundary $B(0, j + 1) = T(0, j)$. Thus, one can calculate $T(0, j)$ as

$$T(0, j) = T(0,0) + \sum_{k=1}^{j} L(0, k). \tag{5}$$

In order to gain analytical understanding, we first study a one dimensional model. Consider a line of consecutive cells $0,1, \ldots, N$. Cell $N$ is the edge cell. Initially cell 0 is frozen. We focus on the growth period $[B(k), T(k)]$ in which cells $0,1, \ldots, k-1$ are frozen and cell

$k$ grows from boundary to frozen. Partial difference equation (2) describes the diffusion dynamics of vapor being transferred from the edge cell to cell $k$. Moreover, cell $k$ accumulates water via addition (1). To derive an analytical solution, we make the following assumption which we justify next.

**Assumption 4.1** For $t \in [B(k), T(k)]$, assume that in the diffusion equation (2), $u_t^+(i) = u_t^-(i)$, for $i = k+1, \dots, N$, and therefore, the vapor distribution reaches a steady state, denoted as $\mu(i|k)$.

From Assumption 4.1, we can ignore the notations of $^-$ and $^+$, and reduce the partial difference equation (2) to the linear equation

$$\mu(i|k) = \frac{1}{2}\big(\mu(i-1|k) + \mu(i+1|k)\big). \tag{6}$$

With the boundary conditions $\mu(k|k) = 0$ and $\mu(N|k) = \beta$, the vapor distribution can be written in a closed form as follows:

$$\mu(i|k) = \frac{i-k}{N-k}\beta, \;\; i = k, \dots, N, \tag{7}$$

which graphically represents a line that connects the two boundary condition points.

We shall now explain why we have made Assumption 4.1. Suppose that the steady state distribution (7) is already reached at $t = B(k)$, i.e., $s_{B(k)}(i) = \mu(i|k-1) = \frac{i-(k-1)}{N-(k-1)}\beta$, for $i = k, \dots, N$. We examine how $s_t(i)$ evolves in the interval of $(B(k), T(k)]$. For $N \gg k$, one has $s_{B(k)}(k) = \mu(k|k-1) = \frac{1}{N-k+1}\beta \approx 0$, and thus it is reasonable to assume $L(k) = T(k) - B(k) \gg 1$ because cell $k$ will take quite a few simulation steps to reach $s_{T(k)}(k) \geq 1$. Moreover, $\left|s_{B(k)}(i) - \mu(i|k)\right| = \left|\frac{i-(k-1)}{N-(k-1)}\,\beta - \frac{i-k}{N-k}\beta\right| \ll 1$ for $N \gg k$. Thus, in each simulation

step of $t \in (B(k), T(k)]$, the function $s_t(i)$ only varies slightly and can be considered approximately constant. Hence, $u_t^+(i) = u_t^-(i)$.

From Equations (2) and (6), we estimate that $\hat{u}_t^+(k) = \frac{\alpha}{4}\frac{1}{N-k}\beta$. Because $u_t^-(k) = 0$, it follows that

$$\Delta\hat{s}_t(k) = \frac{\alpha}{4}\frac{1}{N-k}\beta + \gamma, \tag{8}$$

$$\hat{L}(k) = \frac{1 - s_{B(k)}(k)}{\Delta\hat{s}_t(k)} = \frac{1 - \frac{1}{N-k+1}\beta}{\frac{\alpha}{4}\frac{1}{N-k}\beta + \gamma}. \tag{9}$$

Figure 4(a) below compares $\Delta s_t(k)$ at cell $k$ determined by the simulation, and $\Delta\hat{s}_t(k)$ predicted by (8) for $t \in [B(k), T(k)]$. Initially $s_t(k) \ll \mu(i|k)$, and $\Delta s_t(k) \gg \Delta\hat{s}_t(k)$. In just about 5 simulation steps, $\Delta s_t(k)$ drops to a flat plateau, which is approximately equal to $\Delta\hat{s}_t(k)$. At any time $t$, one observes that $\Delta\hat{s}_t(k) \leq \Delta s_t(k)$. Figure 4(b) compares $L(k)$ determined by the simulation, and $\hat{L}(k)$ predicted by (9) as the snowflake grows from cell 0 to the edge cell. For any $k$, one observes that $L(k) < \hat{L}(k)$. This phenomenon is expected from the following proposition.

**Proposition 4.1** There exists $\alpha > 0$ such that at any time instance $t \in [B(k), T(k)]$, for $i = k, \ldots, N$, $\mu(i|k) \leq s_t(i)$ and $\Delta\hat{s}_t(k) \leq \Delta s_t(k)$. As a result, $\hat{L}(k) \geq L(k)$.

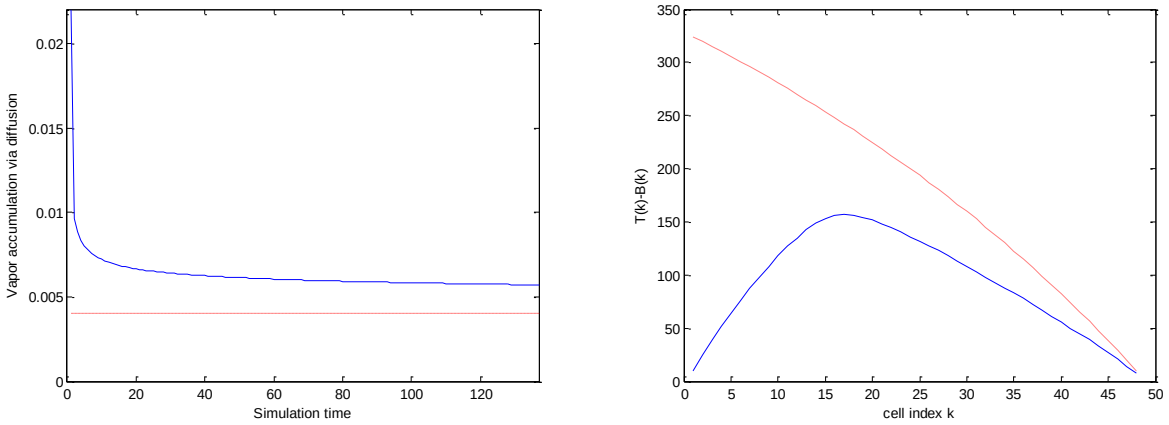


Figure 4. In the one dimensional model with $N = 50$, the left figure (a) compares vapor accumulation in every simulation step, as the simulation proceeds from the time when cell $k = 25$ just becomes boundary to the time when it becomes frozen; the right figure (b) plots $L(k) = T(k) - B(k)$ as a function of cell index. The blue curve is generated by simulating (2) and the red curve is predicted by the steady state model (7). In both pictures, $\alpha = 1, \beta = 0.4, \gamma = 0.001$.

Equation (9) predicts that $\hat{L}(k)$ drops monotonically with $k$. In simulation, we observe that in the beginning the cells grow from boundary to frozen very quickly, well before the steady state is reached. As a result, the steady state assumption 4.1 does not hold in that time period. Figure 4(b) shows that $L(k)$ first increases, then drops, and eventually matches the prediction $\hat{L}(k)$.

Finally, we return to the two dimensional hexagonal cellular case. With a similar steady state assumption, we can reduce the partial difference equation to a set of linear equations similar to Equation (6). However, the geometric structure is much more complex than the one dimensional case. As a result, it is difficult to derive a closed form formula of the vapor distribution similar to (7). Figure 5 below plots $L(0, j)$ along a main branch. Comparison with Figure 4(b) indicates a similarity between the one dimensional and two dimensional cases in that $L$ increases as the snowflake grows from the origin. However, in the two dimensional case, we observe that $L(0,10) = L(0,11) = \cdots = L(0,195)$. When the snowflake grows close to the edge cell, it experiences some edge effect in the simulation where $L$ drops drastically. This indicates

that somewhat surprisingly $\Delta s_t(0,j)$ remains almost constant as the snowflake grows along the main branch.

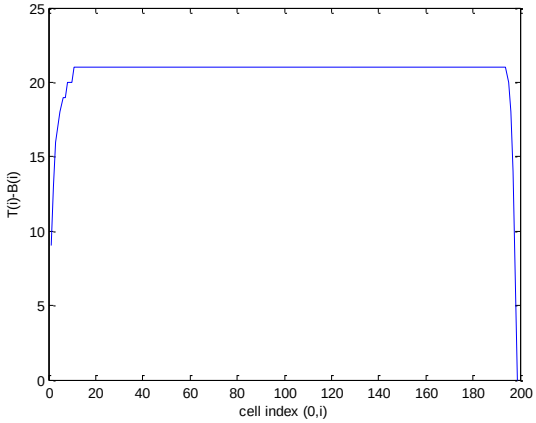


Figure 5. $T(0,j) - B(0,j)$ of cells $(0,j)$ along a main branch for $j = 1,2,\ldots$, in the two dimensional scenario. Cell $(0,200)$ is an edge cell and $\alpha = 1, \beta = 0.4, \gamma = 0.001$.

## 5. Growth of side branches

While the main branches of snowflakes represent clean six fold symmetry, the side branches exhibit characteristic features of chaotic dynamics: complexity and unpredictability. Reiter's model is completely deterministic with no noise or randomness involved, and yet the resultant snowflake images are sensitive to the parameters $\alpha, \beta,$ and $\gamma$ in a chaotic manner. Chaos may appear to be the antithesis of symmetry and structure. Our goal in this section is to discover growth patterns that emerge from seemingly chaotic dynamics.

**Definition 5.1** Starting from a cell $z_0$ on the $j$-axis main branch, the set of consecutive frozen cells in the $i$-axis direction are referred to as *side branch from cell* $z$, and are denoted by $\Phi(z_0) := \{z_0, \ldots, z_{E(z_0)}\}$. Denote by $z_{E(z_0)}$ the outmost cell or *tip*, and by $E(z_0)$ the length of the side branch.

In what follows, we study the growth latency of side branches. Figure 6 below plots the tips of the side branches that grow from the $j$-axis main branch using the parameters of the four images in Figure 2. Due to the chaotic dynamics, the lengths of the side branches vary drastically

with $z_0$ in a seemingly random manner. For image (a), most of the side branches are short and only a small number stand out. The opposite holds for image (d). The scenarios are in between for images (b) and (c). The length of the side branches is indicative of the growth latency. The long side branches represent the ones that grow fastest. In Figure 6 we connect the tips of the long side branches to form an envelope curve that represents the frontier of the side branch growth. The most interesting observation is that the envelope curve can be closely approximated by a straight line for the most part. Recall that the growth latency of the main branch is a constant. Thus we infer that the growth latency of the long side branches is also constant. Denote by $L_M$ and $L_S$ the growth latencies of the main and long side branches respectively. We can show that

$$\frac{L_M}{L_S} = \frac{\sin\left(\frac{2\pi}{3} - \theta\right)}{\sin\theta}, \tag{10}$$

where $\theta$ is the angle between the envelope curve straight line and the $j$-axis. As a specific example, for the magenta curve, the envelope curve of the long side branches grows almost as fast as the main branch such that $\theta \cong \frac{\pi}{3}$ and the resultant image (Figure 2(d)) is roughly a hexagon.

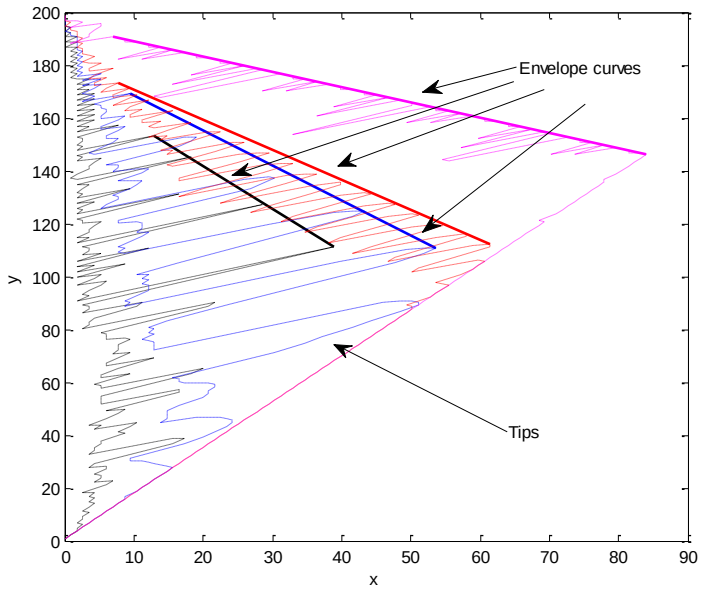


Figure 6. Plots of the tips (thin curves) and envelope curves (thick curves) of the side branches from the $j$-axis main branch using the parameters of the four example images in Figure 2. Due to symmetry, we focus on one set of side branches that grow from the right side of lattice $j$-axis. Here, the black curve represents Figure 2(a), blue for Figure 2(b), red for Figure 2(c), and magenta for Figure 2(d). The $x$-/$y$- axes are the horizontal and vertical axes of the coordinate system.

Next, we study the growth directions of the cells on side branches. Figure 7 below plots the trace of $g$ as a snowflake develops in the simulation. The corresponding snowflake image is shown in Figure 2(b). When a cell $z$ becomes boundary, we mark the cell to indicate $g(z)$ using the legend labeled in the figure. If a cell never becomes boundary, no mark is made. All side branches grow from the $j$-axis main branch, starting in the direction parallel to the $i$-axis. Subsequently, a side branch may split into multiple directions. Indeed, all six orientations have been observed and the dynamics appear chaotic as $g(z)$ appears unpredictable. However, we do find an interesting pattern described below.

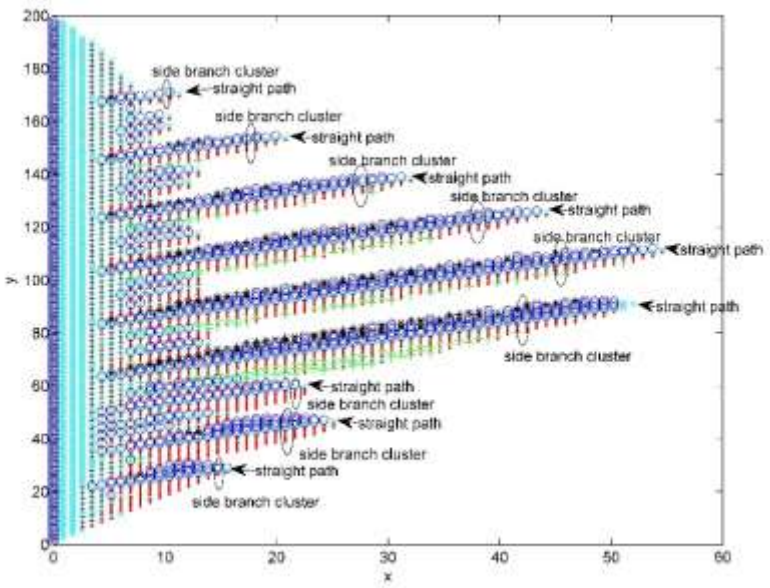


Figure 7. Trace of relative orientations of source cells with respective destination cells. A destination cell becomes boundary because a source cell, which is one of the neighbors of the destination cell, becomes frozen. Legend is as follows: magenta■: $+30°$, black∗: $-30°$, green+: $+90°$, blue∘: $-90°$, red∶ $+150°$, cyan×: $-150°$. $\alpha = 1, \beta = 0.35, \gamma = 0.001$. Not all straight paths are labeled. The $x$- and $y$- axes are the horizontal and vertical axes of the coordinate system Figure 3(a).

**Definition 5.2** Starting from a cell $z_0$ on the $j$-axis main branch, the set of consecutive frozen cells in the $i$-axis direction such that $z_{i-1} = S(z_i)$ for $i = 1,2, \dots, F(z_0)$, are called *straight path* from cell $z$, and are denoted by $\Psi(z_0) := \{z_0, z_1, z_2, \dots, z_{F(z_0)}\}$. Its length is denoted by $F(z_0)$.

Comparison between Definitions 5.1 and 5.2 shows that $\Psi(z_0) \subseteq \Phi(z_0)$ and $F(z_0) \leq E(z_0)$. When a cell $z_{i-1}$ on the straight path becomes frozen, it triggers not only $z_i$ in the $i$-axis direction but also other neighbors to become boundary, resulting in growth in other directions, called *deviating paths*. The straight and deviating paths collectively form a side branch cluster.

**Definition 5.3** A *side branch cluster*, denoted by $\Theta(z_0)$, is the set of frozen cells that can be traced back to a cell on the straight path from cell $z_0$ on the $j$-axis main branch.

Figure 8 below compares the concepts of main branch, side branch, straight path, deviating path, and side branch cluster.

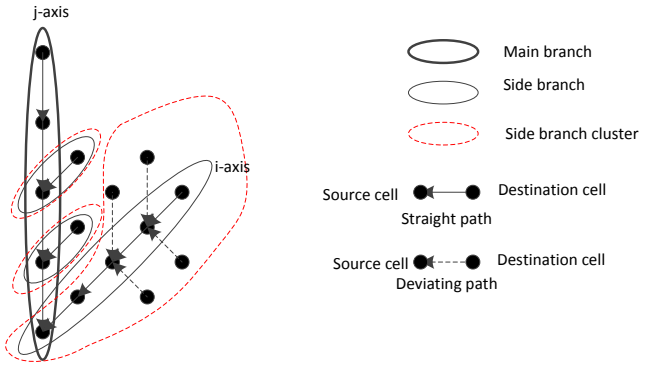


Figure 8. Summary of the concepts of main branch, side branch, straight path, deviating path, and side branch cluster. An arrow linking two cells indicates the source/destination relationship.

A side branch cluster is a visual notion of a collection of side branches that appear to grow together. Figure 7 shows several side branch clusters and the cells on the corresponding straight path marked with cyan ×. Compared with the straight paths, the deviating paths do not grow very far, because they compete with other straight or deviating paths for vapor accumulation in diffusion. On the other hand, the competition with the deviating paths slows down or may even block the growth of a straight path. When a straight path is blocked, the straight path is a strict subset of the corresponding side branch. This scenario is illustrated in Figure 8, where three side branches are shown. The straight path of the middle side branch is blocked by a deviating path of the lower side branch, which grows into a sizeable side branch cluster. We can show this proposition.

**Proposition 5.1** If there exists $z$ such that $z \in \Theta(z_0)$ and $z \notin \Phi(z_0')$, then $\Psi(z_0') \subset \Phi(z_0')$.

**Definition 5.4** Denote by $D(z, z_0)$ the distance between $z_0$ and $z \in \Theta(z_0)$, defined as the smallest number of hops on the lattice from $z$ to $z_0$. Define the length of $\Theta(z_0)$ as $\mathcal{D}(z_0) := \max_{z \in \Theta(z_0)} D(z, z_0)$.

The proposition below states that the straight path determines the length of the side branch cluster.

**Proposition 5.2** There exist $z_1, \dots, z_K \in \Theta(z_0)$, for $K \geq 2$, such that $D(z_k, z_0) = \mathcal{D}(z_0)$ for $k = 1, \dots, K$. Moreover, there exists $i$ with $1 \leq i \leq K$ such that $z_i \in \Psi(z_0)$, and thus $\mathcal{D}(z_0) = F(z_0)$.

## 6. An enhanced Reiter's model

Plates and dendrites are two basic types of regular, symmetrical snowflakes. We observe that while the dendrite images in Figure 2(a)(b) generated by Reiter's model resemble quite accurately the real snowflake in Figure 1(a), as seen in Figure 2 (c)(d) and Figure 1(b)(c), the plate images differ significantly. The plate images in Figure 2(c)(d) is in effect generated as a very leafy dendrite. The reason that Reiter's model is unable to generate plate images *natively* is that the model only takes into account *diffusion*, not taking into account the effect of *local geometry*.

As described in [1], two basic types of mechanisms contribute to the solidification process of snowflakes: diffusion control and interface control. Diffusion control is a nongeometric growth model, where snowflake surfaces are everywhere rough due to diffusion instability, a characteristic result of chaotic dynamics. For example, if a plane snowflake surface develops a small bump, it will have more exposure into the surrounding vapor and grow faster than its immediate neighborhood thanks to diffusion. Interface control is a geometric growth model where snowflake growth only depends on local geometry, i.e., curvature related forces. In the small bump example, the surface molecules on the bump with positive curvature have fewer nearest neighbors than do those on a plane surface and are thus more likely to be removed, making the bump move back to the plane. Interface control makes snowflake surfaces smooth and stable, and it is illustrated in Figure 9 below.

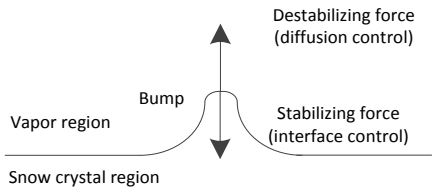


Figure 9. An example showing two competing forces of diffusion control and interface control that determine snowflake growth.

In summary, snowflake growth is determined by the competition of the destabilizing force (diffusion control) and stabilizing force (interface control). In the absence of interface control, Reiter's model is unable to simulate certain features of snowflake growth.

The interface between the snowflake and vapor regions has potential energy, called surface free energy, due to the unfilled electron orbitals of the surface molecules. The surface free energy as a function of direction $\mathbf{n}$, $\gamma(\mathbf{n})$, is determined by the internal structure of snowflake, and in the case of a lattice plane, is proportional to lattice spacing in a given direction. Figure 10(a) below plots the surface free energy $\gamma(\mathbf{n})$ of a snowflake as a function of the direction $\mathbf{n}$. The equilibrium shape of the interface is the one that minimizes the total surface free energy for a given enclosed volume. Wulff construction (see [1]) can be used to derive the equilibrium crystal shape $\mathcal{W}_\gamma$ from the surface free energy plot $\gamma(\mathbf{n})$:

$$\mathcal{W}_\gamma := \{\mathbf{r} | \mathbf{r} \cdot \mathbf{n} \leq \gamma(\mathbf{n}), \forall \mathbf{n}\}. \tag{11}$$

Wulff construction states that the distances of the equilibrium crystal shape from the origin are proportional to their surface free energies per unit area. Figure 10(a) plots the equilibrium crystal shape of snowflake. Moreover, it shows that due to interface control, snowflake growth is the slowest along the lattice axes, and the fastest along the 30°-offset lattice axes.

This can be explained intuitively. Snowflake grows by adding layers of molecules to the existing surfaces. The larger the spaces between parallel lattice planes, the faster the growth is in

that direction. This effect is completely opposite to the diffusion control we have studied in Section 4, where snowflake grows fastest along the lattice axes. This is an example of competition between diffusion control and interface control.

We next propose a new geometric rule to incorporate interface control in Reiter's model. The idea is that the surface free energy minimization forces the lattice points on an equilibrium crystal shape to possess the same amount of vapor so that the surface tends to converge to the equilibrium crystal shape as snowflake grows. From Figure 10(a), we learn that the equilibrium crystal shape is a hexagon except for six narrow regions along the 30°-offset lattice axes where the transition from one edge of the hexagon to another edge is smoothened. The equilibrium crystal shape used in the new geometric rule is shown in Figure 10(b). For a given cell $z_0$, define two *interface control neighbors* $z_0^1, z_0^2$, which are two neighboring cells of $z_0$ on the same equilibrium crystal shape. Figure 10(b) shows the equilibrium crystal shape used in the new geometric rule and the interface control neighbors of the cells. As an example, cells $A, B, C, D, E, F$ are on the same equilibrium crystal shape. Cells $F, B$ are the interface control neighbors of $A$, cells $A, C$ are the interface control neighbors of $B$, etc.

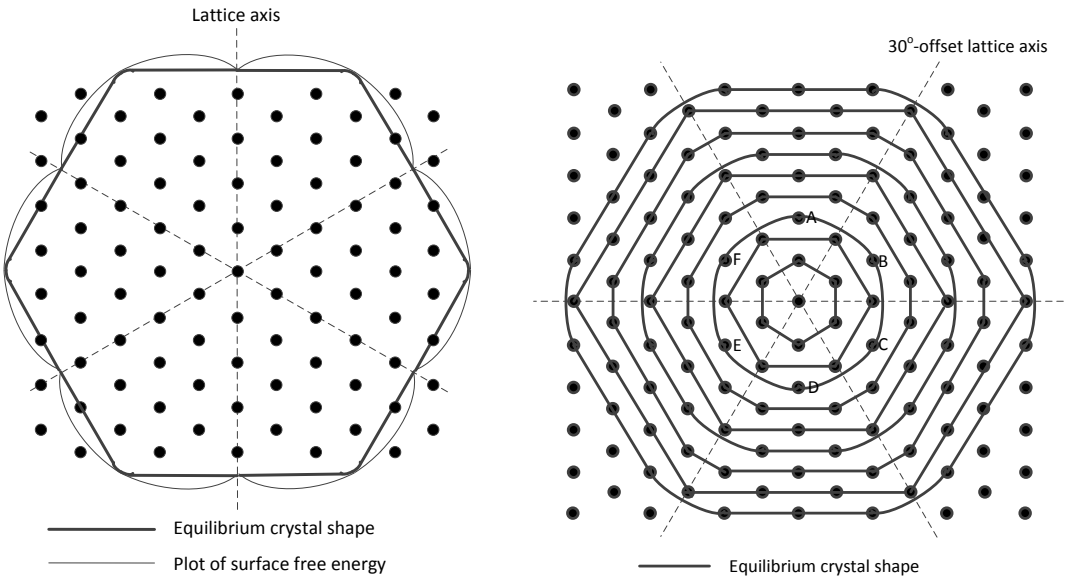


Figure 10. (a) Surface free energy of snowflake as a function of direction and equilibrium crystal shape of snowflake derived from surface free energy plot with Wulff construction [1]. (b) Equilibrium crystal shape used in the new geometric rule.

The new geometric rule is applied after Equation (4) of $s_{t+1}^{-}(z) = u^{+}(z) + v^{+}(z)$. A new variable $\delta_t(z)$ is defined to represent the amount of water to be redistributed for cell $z$ at time $t$. We initialize $\delta_t(z) = 0$ for all $z$. Define $\bar{s}(z_0)$ as the average of the water amounts in cell $z_0$ and its two interface control neighbors $z_0^1, z_0^2$:

$$\bar{s}(z_0) := \frac{1}{3}\left(s_{t+1}^{-}(z_0) + s_{t+1}^{-}(z_0^1) + s_{t+1}^{-}(z_0^2)\right). \tag{12}$$

For every boundary $z_0$, if neither of $z_0^1, z_0^2$ are frozen, then adjust $\delta_t(z_0)$ as follows

$$\delta_s(z_0) = \delta_s(z_0) + \varepsilon\left(\bar{s}(z_0) - s_{t+1}^{-}(z_0)\right), \tag{13}$$

$$\delta_s(z_0^1) = \delta_s(z_0^1) + \varepsilon\left(\bar{s}(z_0) - s_{t+1}^{-}(z_0^1)\right), \tag{14}$$

$$\delta_s(z_0^2) = \delta_s(z_0^2) + \varepsilon\left(\bar{s}(z_0) - s_{t+1}^{-}(z_0^2)\right), \tag{15}$$

After $\delta_s(z)$ has been adjusted for all $z$ according to (13)-(15), finally, for every cell $z$, set

$$s_{t+1}^{+}(z) := s_{t+1}^{-}(z) + \delta_s(z). \tag{16}$$

In (13)-(15), the amount of interface control is determined by $\varepsilon$. Recall that in the original Reiter's model, once water is accumulated in a boundary cell, water stays permanently in that

cell. The new function (16) forces water redistribution particularly among boundary cells to smoothen the snow vapor interface. Figure 11 below shows two snowflake images generated by the enhanced Reiter's model with the new geometric rule.

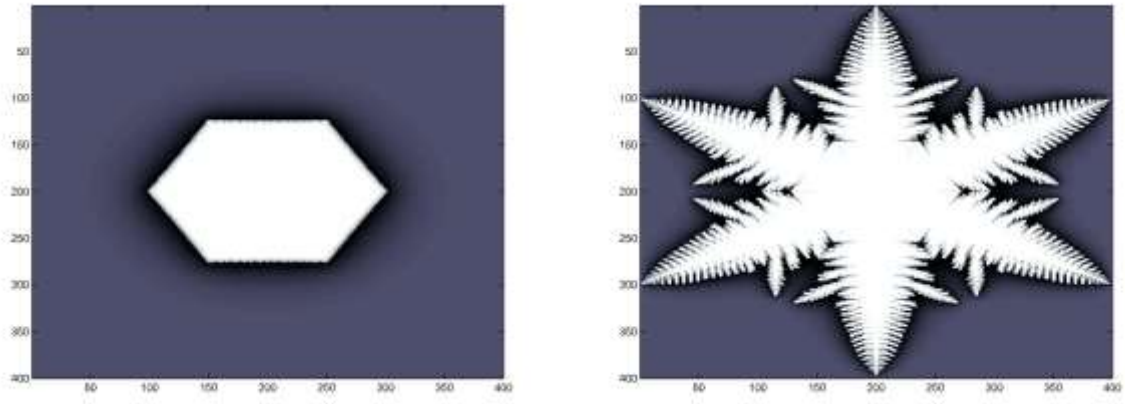

Figure 11. Snowflake images generated by the enhanced Reiter's model with the new geometric rule. (a) $\varepsilon = 0.1$. (b) $\varepsilon = 0.01$. $\alpha = 1, \beta = 0.4, \gamma = 0.001$.

At $\varepsilon = 0.1$, the image resembles a plate observed in nature much more closely than the ones in Figure 2. By reducing interface control with $\varepsilon = 0.01$, the snowflake starts as a plate and later becomes a dendrite as diffusion control dominates interface control.

## 7. Conclusions and future work

In this paper we have analyzed the growth of snowflake images generated by a computer simulation model (Reiter's model [11]), and have proposed ways to improve the model. A snowflake consists of main branches and side branches. We have derived an analytical solution of the main branch growth latency and made numerical comparison with simulation results. We have discovered interesting patterns of side branches in terms of growth latency and direction. Finally, to enhance the model, we have introduced a new geometric rule that incorporates interface control, a basic mechanism of the solidification process, which is not present in the original Reiter's model.

In follow up work, we shall further investigate some interesting patterns observed in this study. On the main branch growth, we will consider why the growth latency is almost constant (Figure 5) and whether this phenomenon is unique to the hexagonal cells or applicable to other two dimensional lattices. On the side branch growth, we have noted that some side branches grow much faster than their neighbors, and that with slightly different diffusion parameters the side branch growth latency could change drastically at the same position while the main branch growth latency remains virtually the same. Our preliminary study shows that this great sensitivity is attributable to diffusion instability – when the growth of cells in some direction gain initial advantage over their neighbors, the advantage continues to expand such that the growth in that direction becomes even faster. We find that diffusion instability is caused by competition among cells in diffusion and the average number of contributing neighbors is a good indicator to explain diffusion instability. Finally, we will use the enhanced model to explore the interplay of diffusion and interface control. For example, we shall simulate growth in an environment where the diffusion and interface control parameters vary with time so as to generate images similar to Figure 1(b)(c). We shall also define quantitative methods to compare the original and enhanced models.

## Acknowledgments

I would like to thank my mentor, Professor Laura Schaposnik of the University of Illinois at Urbana-Champaign. She introduced me to the general field of snowflake modeling, provided direction in my research, and informed me of the connection between my work and chaos theory. I would like to thank Dr. Thaler, postdoctoral research associate at the University of Illinois at Urbana-Champaign, for suggesting that to rigorously prove that the main branches grow the fastest and the offset branches grow the slowest, I should pursue finite element analysis of crystal growth and formation. I would like to thank MIT PRIMES and Illinois Geometry Lab for giving me the opportunity and resources to work on this project.

## References

[1] John A Adam, Flowers of ice beauty, symmetry, and complexity: A review of the snowflake: Winter's secret beauty. *Notices Amer. Math. Soc*, 52:402 − 416, 2005.

[2] Janko Gravner and David Griffeath, Modeling snowflake growth II: A mesoscopic lattice map with plausible dynamics. *Physics D: Nonlinear Phenomena*, 237(3): 385 − 404, 2008.

[3] Janko Gravner and David Griffeath, Modeling snowflake growth III: A three-dimensional mesoscopic approach. *Phys. Rev. E*, 79:011601, 2009.

[4] Kenneth G. Libbrecht, The physics of snowflakes. *Rep. Prog. Phys.*, 68:855 − 895, 2005.

[5] Kenneth G. Libbrecht, A guide to snowflakes. http://www.its.caltech.edu/~atomic/snowcrystals/class/class.html, 2014.

[6] C. Magono and C.W. Lee, Meteorological classification of natural snowflakes. *Journal of the Faculty of Science, Hokkaido University*, 1966.

[7] B. Mason, *The Physics of Clouds*. Oxford University Press, 1971.

[8] U. Nakaya, *Snowflakes: Natural and Artificial*. Harvard University Press, 1954.

[9] C. Ning and C. Reiter, A cellular model for 3-dimensional snowflakelization. *Computers and Graphics*, 31:668 − 677, 2007.

[10] N. H. Packard, Lattice models for solidification and aggregation. Institute for Advanced Study preprint, 1984. Reprinted in Theory and Application of Cellular Automata, S. Wolfram, editor, World Scientific, 1986, 305 − 310.

[11] C. Reiter, A local cellular model for snowflake growth. Chaos, Solitions & Fractals, 23:1111 − 1119, 2005.

[12] T. Wittern and L. Sander, Diffusion-limited aggregation, a kinetic critical phenomenon. *Phys. Rev. Lett.*, 47:1400 − 1403, 1981.